

## Direct magneto-optical measurements of anisotropic critical currents in $(\text{La}_{1-x}\text{Sr}_x)_2\text{CuO}_4$ single crystals

C. A. Durán, P. L. Gammel, R. Wolfe, V. J. Fratello, and D. J. Bishop  
*AT&T Bell Laboratories, Murray Hill, New Jersey 07974*

T. Kimura, K. Kitazawa, and K. Kishio  
*University of Tokyo, Bunkyo-ku, Tokyo 113, Japan*  
(Received 27 September 1993)

We report on measurements of the penetration of magnetic flux in single crystals of  $(\text{La}_{1-x}\text{Sr}_x)_2\text{CuO}_4$  as seen using the magnetic garnet imaging technique. The technique measures the spatial and temporal dependence of the magnetization by using a wafer of doped magnetic garnet material placed in contact with the sample to be measured and imaged with an optical microscope. We have directly measured the critical current anisotropy in this system as a function of temperature and doping and found clear evidence for intrinsic pinning as well as a pronounced dependence of the anisotropy on doping.

An understanding of the behavior of critical currents in the copper-oxide superconductors will be crucial to many of the envisioned applications for these materials as well as being of importance to a fundamental understanding of the superconducting state itself. The crucial role that the anisotropic nature of these materials plays in this area is already widely acknowledged. For example, the anisotropy of the in-plane critical currents<sup>1</sup> has been demonstrated in thin films of Y-Ba-Cu-O in which it is possible to use  $I$ - $V$  methods. However, in thin-film samples, it is not, in general, possible to measure out-of-plane critical currents unless specially grown samples<sup>2</sup> are used and then it is not obvious that the observed behavior will match that of bulk, single crystals. This is unfortunate because the out-of-plane critical current anisotropies are expected to demonstrate some of the most interesting and important effects. In addition, transport measurements become difficult when the critical currents are very high requiring the use of magnetic methods. However, the averaging nature of most magnetic techniques requires significant modeling<sup>3</sup> to allow one to extract the anisotropic critical currents from several sets of data and they render such techniques completely incapable of determining whether the observed behavior is due to the bulk material or is dominated by defects. For example, there is significant evidence that in the Y-Ba-Cu-O system, the decay of the magnetization in a bulk sample can be completely dominated by the effect of the twins.<sup>4</sup> Also, there are regimes in which the magnetization can form non-trivial spatial patterns which will be missed entirely by a transport technique or a measurement of the averaged magnetic properties. Thus, we feel that there can be significant advantages in using *spatially resolved* magnetic techniques to extract the behavior of the anisotropic critical currents in these systems.

In this paper we report on a direct observation of the anisotropic magnetic-field penetration in large, single crystals of  $(\text{La}_{1-x}\text{Sr}_x)_2\text{CuO}_4$  as a function of temperature

and doping. From our data, we can directly extract the critical current anisotropies without the need to make any assumptions about the magnetic field distribution in the sample. Our measurements find a significant critical current anisotropy in this system which increases with increasing temperature suggesting that the intrinsic pinning is robust.<sup>1,5</sup> In addition, we find that the critical current anisotropy decreases rapidly with increased doping, a result consistent with the doping dependence found for the anisotropic effective-mass ratio.<sup>6,7</sup>

Our samples were rectangular slabs of  $(\text{La}_{1-x}\text{Sr}_x)_2\text{CuO}_4$  which were cut from large single crystals grown by a traveling solvent floating zone method as described in Refs. 6 and 8. The crystals we used had compositions for which  $x = 0.05, 0.08$ , and  $0.1$ . The superconducting critical temperatures were measured using standard magnetization techniques and found to be 27, 36, and 30.5 K, respectively, for the three compositions. From each crystal, after x-raying to determine the orientation, we cut two samples, which were then mechanically polished on two mutually parallel faces. In one sample of each pair, the polished faces were chosen to be parallel to the copper-oxide planes in the crystal structure and for the other sample of each pair, the polished faces were chosen to contain the crystalline  $c$  axis and thus were perpendicular to the conducting planes. Typical dimensions for our samples were a few hundred  $\mu\text{m}$  in the direction perpendicular to the polished faces and several mm in the other two directions.

Our measurement technique uses an epitaxially grown magnetic garnet film which is placed next to the superconducting sample we wish to measure. These Bi-doped iron garnet films have ferrimagnetically ordered domains and are highly anisotropic resulting in a local magnetization which is always perpendicular to the plane of the film. When the external applied field is zero, roughly half of the domains will point "up" and the other half "down." The domains can be imaged using a polarized

light microscope since the domains will rotate the polarization of transmitted light through the garnet and the up and down domains can then be seen as light and dark regions. When a magnetic field is applied, the relative population of up and down domains changes in a way proportional to the perpendicular component of that field. At low enough fields, this change is linear in field and by using a CCD camera and a computer system, it is possible to measure the local magnetic field variations by looking at the local gray scale.<sup>4</sup> Our technique has a field sensitivity of approximately 1 G in the optimal configuration and a spatial resolution of several magnetic domains or  $\sim 5 \mu\text{m}$ . A more complete description of our experimental technique can be found in Ref. 4.

The upper panel of Fig. 1 shows a contour plot of the magnetic-field distribution obtained as described above on the  $a$ - $c$  face of a sample with  $x=0.08$ , at a temperature of 5 K and with an oscillating ( $f \sim 1$  Hz) magnetic field of 50 G applied. The field scale is shown as an inset to the figure. The anisotropy of the critical current is clearly apparent in this picture. The lower critical current in the  $c$  direction is responsible for the preferential penetration of the flux perpendicular to it as seen by the larger spacing between the constant field lines in the figure. In Figs. 1(b) and 1(c) are shown field profiles measured from the data in Fig. 1(a) along the  $c$  and  $a$  directions. The field profiles in Figs. 1(b) and 1(c) were plotted using the full set of data points, and not an averaged subset as the two-dimensional plot of Fig. 1(a).

Within the framework of a Bean model<sup>9</sup> type of analysis, one could try to measure the critical current anisotropy by measuring the field slopes in the lower two figures. However, due to the highly demagnetized nature of our samples, it would be incorrect to directly compute the critical currents from this measured field slope. Moreover, even if our samples were thicker, the field lines would still be strongly curved near the surface, making such a simple procedure inadequate. Our technique for extracting the critical currents from our measurements is similar to the one used previously by Daumling and Larbarlestier<sup>10</sup> but using our specific sample geometry. The field profiles are computed as the superposition of a uniform applied field and the spatially modulated field caused by the shielding currents. The data are then compared with this calculated normal field distribution giving us the critical currents for each sample. For the purpose of our computations, we assume that the sample is infinite in the direction perpendicular to the profile which is being computed while the actual sample sizes were used for the other two dimensions. This simplification reduced the running time of our computations by an order of magnitude and was checked and found to produce a systematic under estimation of the critical currents of less than 5%. Qualitatively, the finite sample length produces profiles which would have a sharper maximum right at the edge of the sample and a tail which decays more rapidly as one moves away from the sample edge, improving the overall quality of the fits.

Other approximations were done in our computations as well. The shielding current was assumed to be characterized by a single critical current density  $J_c$ , flowing uni-

formly across the sample thickness in from the edge to a finite thickness  $d$  and zero from that depth to the center of the sample. This hollow geometry for the current distribution is schematized at the top of Fig. 1(c) and is responsible for the shallow maximum that the corresponding computed field has at the center of the sample. This maximum is not found in the real data as additional currents flow in the sample in order to prevent this from happening. A current distribution closer to the real one should incorporate these currents. To evaluate this situation, we have added a second layer of uniform current flow placed adjacent to the current layer responsible for

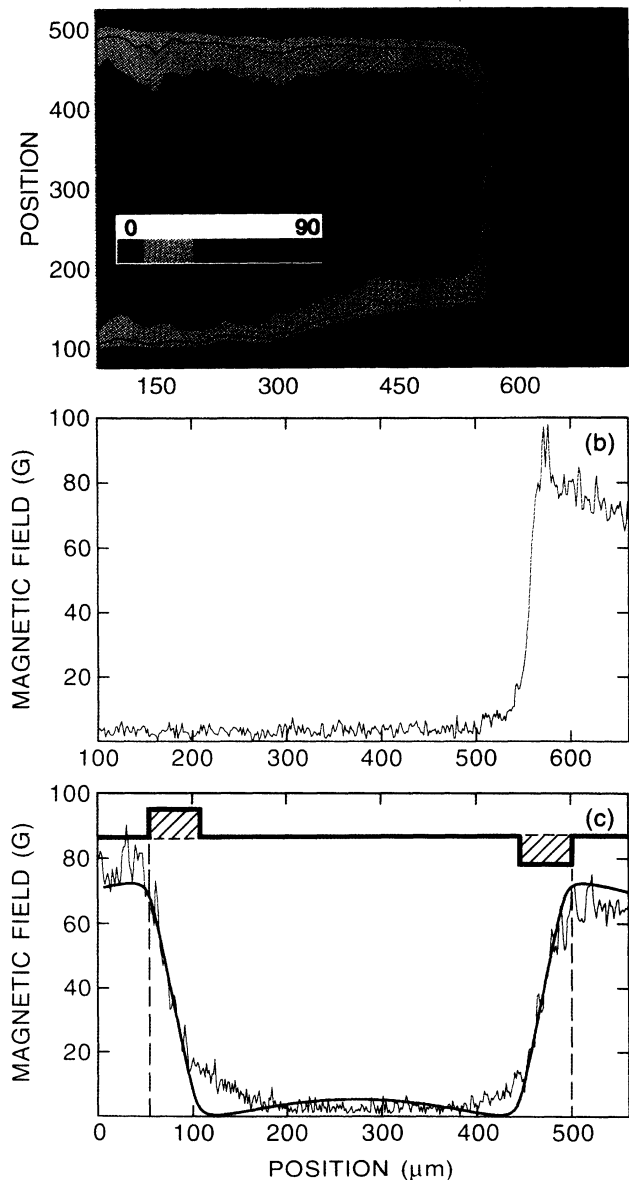


FIG. 1. (a) Contour plot of the magnetic-field penetration on an  $a$ - $c$  face of the sample with  $x=0.08$ . The crystalline  $a$  axis is vertical,  $c$  is horizontal, and  $b$  is out of the plane of the page. (b) Field profile taken along a horizontal line in the plot of (a). (c) Field profile taken along a vertical line in (a). The solid line is a fit (see text). The thick line at the top schematizes the current distribution used in the fit.

most of the shielding. This has the effect of progressively suppressing the central maximum while generating two shoulders localized near the sample edges [see Fig. 1(c)]. Of course, in order to conserve the total current, the main shielding current density has to be reduced. This tedious process of fine tuning the current distribution while increasing the number of fitting parameters was done in only one case in order to evaluate the systematic errors inherent in the simpler fitting process. The assumption of a single current flow produced a systematic overestimation of the critical current density which was on the order of a few percent. To some extent, the systematic errors tended to cancel.

For the fitting of the measured profiles, we varied two quantities  $J_c$  and  $d$ . These two quantities cannot be varied independently because the product  $J_c d$  ( $t$  is the sample thickness) must produce the total shielding current,  $I_t$ . While  $J_c$  determines the profile slope,  $I_t$  must

be fixed by the difference in field between the center of the sample and the external applied field. To check the validity of a constant  $J_c$ , we have tested the consistency of our data by taking data at a constant temperature with different applied fields and fit the differing profiles by changing only  $d$ . A further check was made by taking data at a fixed applied field and varying the temperature and performing the fits with a constant  $I_t$ . The results of all of our fits for the anisotropic critical currents are shown in Fig. 2.

In Fig. 2(a) we show the in-plane critical currents  $J_c^{ab,c}$  for three dopings as measured for the case of  $H \parallel c$ . (In our notation for  $J_c$ , the first superscript represents the current direction and the second the field direction. As we will show below, the intrinsic pinning in this system requires us to use this complex notation.) Figures 2(b) and 2(c) show the measured values of  $J_c^{ab,ab}$  and  $J_c^{c,ab}$ , respectively, measured with the field in the plane. As shown in Fig. 2(a), the in-plane critical current density,  $J_c^{ab,c}$  is maximized for the optimal doping and is depressed both for under- and overdoping with Sr. Also notice that  $J_c^{ab,c}$  and  $J_c^{ab,ab}$  are different as shown in Figs. 2(a) and 2(b). Thus, there is a strong intrinsic pinning effect in this system, i.e., the vortices are pinned by the copper-oxide planes and  $J_c^{ab,ab}$  is greater than  $J_c^{ab,c}$ . We find that this intrinsic pinning effect as measured by the ratio of  $J_c^{ab,ab}/J_c^{ab,c}$  is minimal for  $x = 0.08$ . This implies that the anisotropic modulation of the superconducting order parameter, which is responsible for intrinsic pinning, attains a minimum at the optimal doping, in contrast with the monotonic behavior observed in the normal-state resistivity anisotropy.

An interesting effect is the one illustrated in Fig. 3 where we have plotted the temperature dependence of the anisotropy ratio  $J_c^{ab,ab}/J_c^{c,ab}$  directly measured with the field parallel to the copper-oxide planes. While the anisotropy ratio for the samples with  $x = 0.08$  and  $0.10$  is roughly the same, for the case of  $x = 0.05$  it is an order of

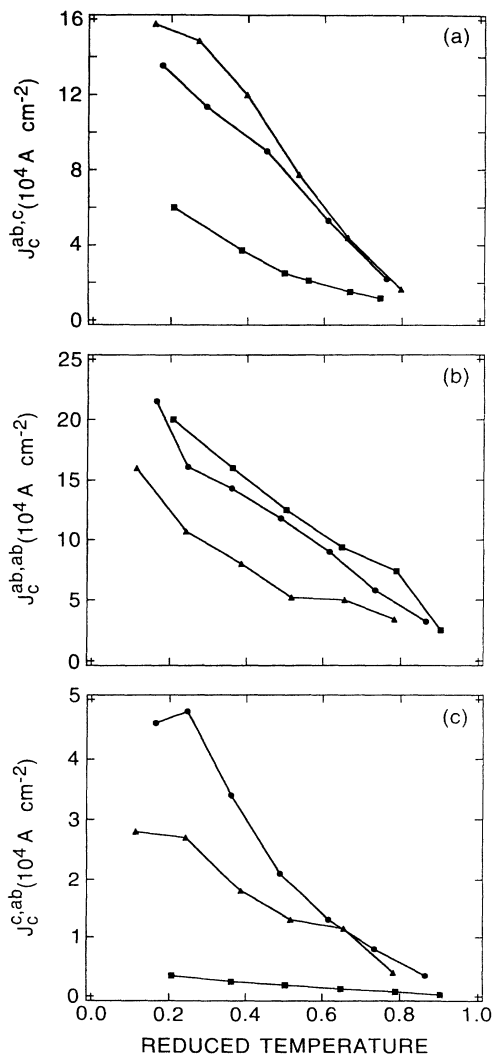


FIG. 2. Shown are the critical currents extracted from our fits to the field profiles measured in different configurations and different samples ( $n$ :  $x = 0.05$ ;  $s$ :  $x = 0.08$ ;  $l$ :  $x = 0.10$ ). The data shown in (a) were obtained for observations on  $a$ - $b$  faces while the ones in (b) and (c) are from  $a$ - $c$  faces.

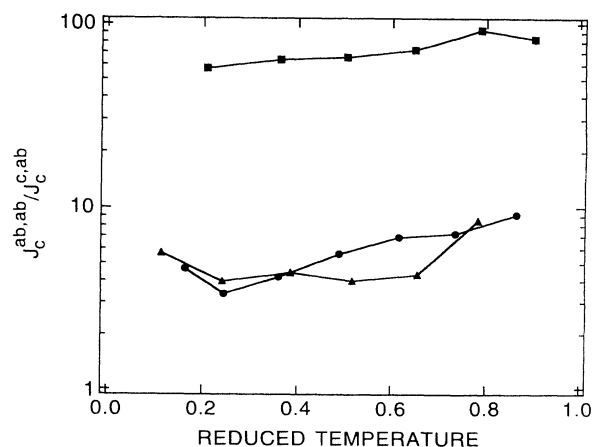


FIG. 3. Shown are the ratios between critical currents as measured on  $a$ - $c$  faces [Figs. 2(b) and 2(c)]. The observed enhancement of the anisotropy with temperature is due to the relative robustness of the intrinsic pinning mechanism. The symbols are as in Fig. 2.

magnitude larger. The anisotropy ratio is temperature dependent for the two samples with doping of  $x = 0.05$  and  $0.10$ , changing roughly 50% between a reduced temperature of 0.2 and 0.8. However, this ratio for the sample with  $x = 0.08$  is essentially temperature independent. This suggests that thermal fluctuations are depressing the out-of-plane critical currents with respect to the ones in the planes. On the other hand, the ratio  $J_c^{ab,c}/J_c^{c,ab}$ , which is not affected by intrinsic pinning, does not show any temperature dependence for the three samples. This indicates that there is a relative enhancement of the intrinsic pinning in this system with increasing temperature. This gives us confidence that the measured critical current densities  $J_c^{ab,c}$  and  $J_c^{c,ab}$  are intrinsic to the ma-

terials and do not arise from the surfaces or geometrical effects.

In conclusion, we have reported on direct measurements of anisotropic critical currents in the  $(\text{La}_{1-x}\text{Sr}_x)_2\text{CuO}_4$  system as a function of doping and temperature. We have found a strong intrinsic pinning effect in this system which depends in a pronounced way on Sr doping. The data show that the intrinsic pinning is more robust than the other relevant pinning mechanisms as the temperature is increased.

The authors would like to acknowledge many useful discussions with John Clem, David Huse, Vladimir Kogan, and Francisco de la Cruz.

<sup>1</sup>B. Roas, L. Schultz, and G. Saemann-Ischenko, *Phys. Rev. Lett.* **64**, 479 (1990).

<sup>2</sup>H. L. Kao *et al.*, *Phys. Rev. B* **48**, 9925 (1993).

<sup>3</sup>E. M. Gyorgy, R. B. van Dover, K. A. Jackson, L. F. Schneemeyer, and J. V. Waszczak, *Appl. Phys. Lett.* **55**, 283 (1989).

<sup>4</sup>C. A. Durán, P. L. Gammel, R. Wolfe, V. J. Fratello, D. J. Bishop, J. P. Rice, and D. M. Ginsberg, *Nature* **357**, 474 (1992).

<sup>5</sup>M. Tachiki and S. Takahashi, *Solid State Commun.* **70**, 291 (1989).

<sup>6</sup>T. Kimura, K. Kishio, T. Kobayashi, Y. Nakayama, N. Motohira, K. Kitazawa, and K. Yamafuji, *Physica C* **192**, 247 (1992); T. Kimura, Master's thesis, University of Tokyo, 1993 (unpublished).

<sup>7</sup>T. Ito, H. Takagi, S. Ishibashi, T. Ido, and S. Uchida, *Nature* **350**, 596 (1991).

<sup>8</sup>I. Tanaka and H. Kojima, *Nature* **337**, 21 (1988).

<sup>9</sup>C. P. Bean, *Phys. Rev. Lett.* **8**, 250 (1962).

<sup>10</sup>M. Daumling and D. C. Larbalestier, *Phys. Rev. B* **40**, 9350 (1989).

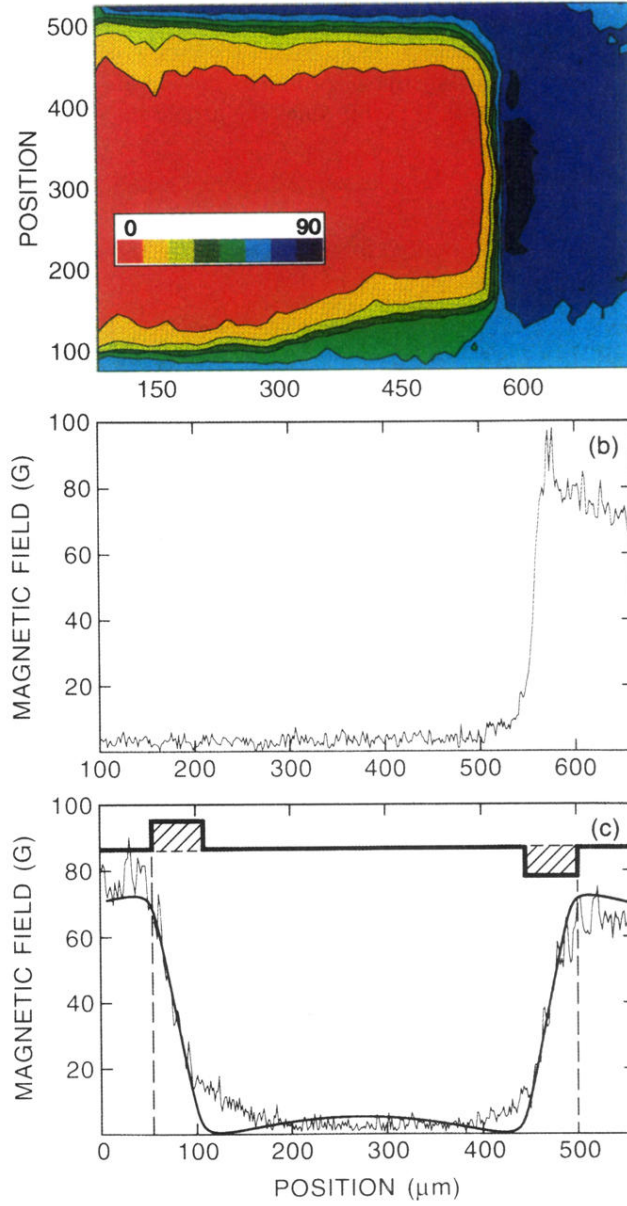


**FIG. 1.** (a) Contour plot of the magnetic-field penetration on an  $a$ - $c$  face of the sample with  $x = 0.08$ . The crystalline  $a$  axis is vertical,  $c$  is horizontal, and  $b$  is out of the plane of the page. (b) Field profile taken along a horizontal line in the plot of (a). (c) Field profile taken along a vertical line in (a). The solid line is a fit (see text). The thick line at the top schematizes the current distribution used in the fit.